Chinese Physical Society | IOP Publishing
CPB
Chinese Physics B
http://cpb.iphy.ac.cn https://iopscience.iop.org/journal/1674-1056

Design of vertical diamond Schottky barrier diode with junction terminal extension structure by using the n-Ga_2O_3/p-diamond heterojunction

Wang Lin(林旺), Ting-Ting Wang(王婷婷), Qi-Liang Wang(王启亮), Xian-Yi Lv(吕宪义),Gen-Zhuang Li(李根壮), Liu-An Li(李柳暗), Jin-Ping Ao(敖金平), and Guang-Tian Zou(邹广田)

Citation: Chin. Phys. B, 2022, 31 (**10**): 108105.   DOI: 10.1088/1674-1056/ac7e37
Journal homepage: http://cpb.iphy.ac.cn; http://iopscience.iop.org/cpb

What follows is a list of articles you may be interested in

Relationship between the spatial position of the seed and growth mode for single-crystal diamond grown with an enclosed-type holder

Wen-Liang Xie(谢文良), Xian-Yi Lv(吕宪义), Qi-Liang Wang(王启亮),Liu-An Li(李柳暗), and Guang-Tian Zou(邹广田)
Chin. Phys. B, 2022, 31 (**10**): 108106.   DOI: 10.1088/1674-1056/ac7e35

Determination of band alignment between GaO_x and boron doped diamond for a selective-area-doped termination structure

Qi-Liang Wang(王启亮), Shi-Yang Fu(付诗洋), Si-Han He(何思翰), Hai-Bo Zhang(张海波),Shao-Heng Cheng(成绍恒), Liu-An Li(李柳暗), and Hong-Dong Li(李红东)
Chin. Phys. B, 2022, 31 (**8**): 088104.   DOI: 10.1088/1674-1056/ac464e

Synergistic influences of titanium, boron, and oxygen on large-size single-crystal diamond growth at high pressure and high temperature

Guang-Tong Zhou(周广通), Yu-Hu Mu(穆玉虎), Yuan-Wen Song(宋元文), Zhuang-Fei Zhang(张壮飞), Yue-Wen Zhang(张跃文), Wei-Xia Shen(沈维霞), Qian-Qian Wang(王倩倩), Biao Wan(万彪), Chao Fang(房超), Liang-Chao Chen(陈良超), Ya-Dong Li(李亚东), and Xiao-Peng Jia(贾晓鹏)
Chin. Phys. B, 2022, 31 (**6**): 068103.   DOI: 10.1088/1674-1056/ac4650

Synthesis and characterizations of boron and nitrogen co-doped high pressure and high temperature large single-crystal diamonds with increased mobility

Xin-Yuan Miao(苗辛原), Hong-An Ma(马红安), Zhuang-Fei Zhang(张壮飞), Liang-Chao Chen(陈良超), Li-Juan Zhou(周丽娟), Min-Si Li(李敏斯), and Xiao-Peng Jia(贾晓鹏)
Chin. Phys. B, 2021, 30 (**6**): 068102.   DOI: 10.1088/1674-1056/abf12c

---

SPECIAL TOPIC — Celebrating the 70th Anniversary of the Physics of Jilin University

Design of vertical diamond Schottky barrier diode with junction terminal extension structure by using the n-Ga_2O_3/p-diamond heterojunction

Wang Lin(林旺)[1,2], Ting-Ting Wang(王婷婷)[3], Qi-Liang Wang(王启亮)[1,2], Xian-Yi Lv(吕宪义)[1,2], Gen-Zhuang Li(李根壮)[1,2], Liu-An Li(李柳暗)[1,2,†], Jin-Ping Ao(敖金平)[3], and Guang-Tian Zou(邹广田)[1,2,‡]

[1] *State Key Laboratory of Superhard Material, College of Physics, Jilin University, Changchun* 130012*, China*
[2] *Shenzhen Research Institute, Jilin University, Shenzhen* 518057*, China*
[3] *National Key Discipline Laboratory of Wide Bandgap Semiconductor, Xidian University, Xi'an* 710071*, China*

(Received 24 May 2022; revised manuscript received 23 June 2022; accepted manuscript online 5 July 2022)

A novel junction terminal extension structure is proposed for vertical diamond Schottky barrier diodes (SBDs) by using an n-Ga_2O_3/p-diamond heterojunction. The depletion region of the heterojunction suppresses part of the forward current conduction path, which slightly increases the on-resistance. On the other hand, the reverse breakdown voltage is enhanced obviously because of attenuated electric field crowding. By optimizing the doping concentration, length, and depth of n-Ga_2O_3, the trade-off between on-resistance and breakdown voltage with a high Baliga figure of merit (FOM) value is realized through Silvaco technology computer-aided design simulation. In addition, the effect of the work functions of the Schottky electrodes is evaluated. The results are beneficial to realizing a high-performance vertical diamond SBD.

Keywords: diamond, Schottky barrier diode, junction terminal extension, simulation

PACS: 81.05.ug,73.30.+y, 85.30.Kk, 88.30.gg **DOI:** 10.1088/1674-1056/ac7e37

1. Introduction

Diamond is a promising material for the next generation power electronic devices because of its low consumption and high-frequency operation. In addition, diamond can be used at high temperature with small leakage current due to its extremely low intrinsic carrier concentration. Compared with conventional power electronic device materials (such as Si, SiC, and GaN), diamond has higher carrier mobilities [4500 $cm^2/(V \cdot s)$ for electrons and 3800 $cm^2/(V \cdot s)$ for holes], higher critical electric field (> 10 MV/cm), higher thermal conductivity [2000 W/(m·K)], lower dielectric constant (5.7), and wide bandgap (5.5 eV).[1,2] The theoretical Baliga figure of merit (BFOM) value of diamond is 23000 (normalized to Si), which means that a diamond-based power electronic device is a promising candidate to balance the on-resistance (R_{on}) and breakdown voltage (V_{BD}).[3,4]

Schottky barrier diodes (SBDs) are the most commonly used electronic component in electric circuits because they have low power loss and no recovery current.[5–10] However, electric field crowding is usually observed in SBDs under a large reverse voltage, which decreases the energy barrier and increases the reverse leakage current seriously. Up to now, various advanced termination structures such as field plates,[11–14] ion implantation,[15–17] and metal guard rings have been adopted to enhance V_{BD}.[18,19] However, some effective termination structures such as junction terminal extension (JTE) and junction barrier Schottky (JBS) structures are still a challenge for diamond due to the lack of n-type doping.[20] A nitrogen dopant shows a large activation energy of 1.7 eV, whereas a phosphorus dopant shows a low doping efficiency (50%–90% compensation ratio).[21]

Recently, wide bandgap gallium oxide (GaO_x) with a bandgap of 4.8 eV and a critical electric field of 8 MV/cm has been adopted to construct n-GaO_x/p-diamond heterojunctions.[22] GaO_x can easily obtain n-type doping (10^{16}–10^{19} cm^{-3}) by optimizing the growth conditions,[23] which is beneficial to realizing high-performance photodiodes. In our previous work,[24] the band configuration of the GaO_x/diamond interface was determined, which has potential for JTE and JBS application. Herein, a vertical diamond SBD with an n-Ga_2O_3 JTE structure was designed by a Silvaco technology computer-aided design (TCAD) software. By optimizing the JTE length, doping concentration, width, and depth of n-Ga_2O_3, the trade-off between on-resistance and breakdown voltage without obvious crowding effect on the Schottky contact characteristics was realized.

2. Device structure and simulations

The vertical diamond SBDs with and without n-Ga_2O_3 JTE were designed through Silvaco TCAD. The cross-

†Corresponding author. E-mail: liliuan@jlu.edu.cn
‡Corresponding author. E-mail: gtzou@jlu.edu.cn

sectional structures of the SBDs are shown in Figs. 1(a) and 1(b). The structure consists of a p^+-diamond substrate (1×10^{19} cm^{-3}, 0.5 μm) and a p^--diamond drift layer (1×10^{16} cm^{-3}, 3.5 μm). The anode and cathode were located at the bottom and top of the device and set into ohmic and Schottky contact, respectively. For the reference diode without JTE (Fig. 1(a)), the length of the cathode electrode was 10 μm. The n-Ga_2O_3 regions were buried beneath the Schottky contact with an overlap of 1.0 μm. Different n-Ga_2O_3 doping concentrations (1×10^{17} cm^{-3}, 5×10^{17} cm^{-3}, 1×10^{18} cm^{-3}, and 5×10^{18} cm^{-3}), JTE lengths L (0 μm, 1.5 μm, 2 μm, 2.5 μm, and 3 μm), and JTE depths D (0 nm, 50 nm, 100 nm, 150 nm, and 200 nm) were used for the simulations. The commonly used parallel electric field–dependent mobility model, the Auger recombination model, the Shockley–Read–Hall model, and the impact ionization model were adopted to obtain the current–voltage (I–V) curve and electric field distribution of the SBDs.[25] In addition, a universal phonon-assisted tunneling model was defined at the anode region. The key material parameters of diamond and Ga_2O_3[26] in the simulations are shown in Table 1. The electron mobility μ_n (hole mobility μ_p) of p^+ diamond, p^- diamond, and n-Ga_2O_3 were 1000 (30) cm^2/(V·s), 1000 (200) cm^2/(V·s), and 200 (50) cm^2/(V·s), respectively. The impact ionization parameters of diamond and Ga_2O_3 are shown in Table 2.

Table 1. Key material parameters of diamond and Ga_2O_3 used in the simulations.

Material	Affinity (eV)	Eg300 (eV)	Nc300 (10^{18})	Nv300 (10^{19})	Permittivity
Diamond	1.5	5.47	5	1.8	5.7
Ga_2O_3	4.0	4.8	3.72	1.16	10.2

Table 2. Impact ionization coefficients of diamond[27] and Ga_2O_3 used in the simulations.[28]

Material	An (10^5)	Ap (10^6)	Bn (10^7)	Bp (10^7)
Diamond	1.89	5.4	1.7	1.42
Ga_2O_3	7.06	0.706	2.1	2.1

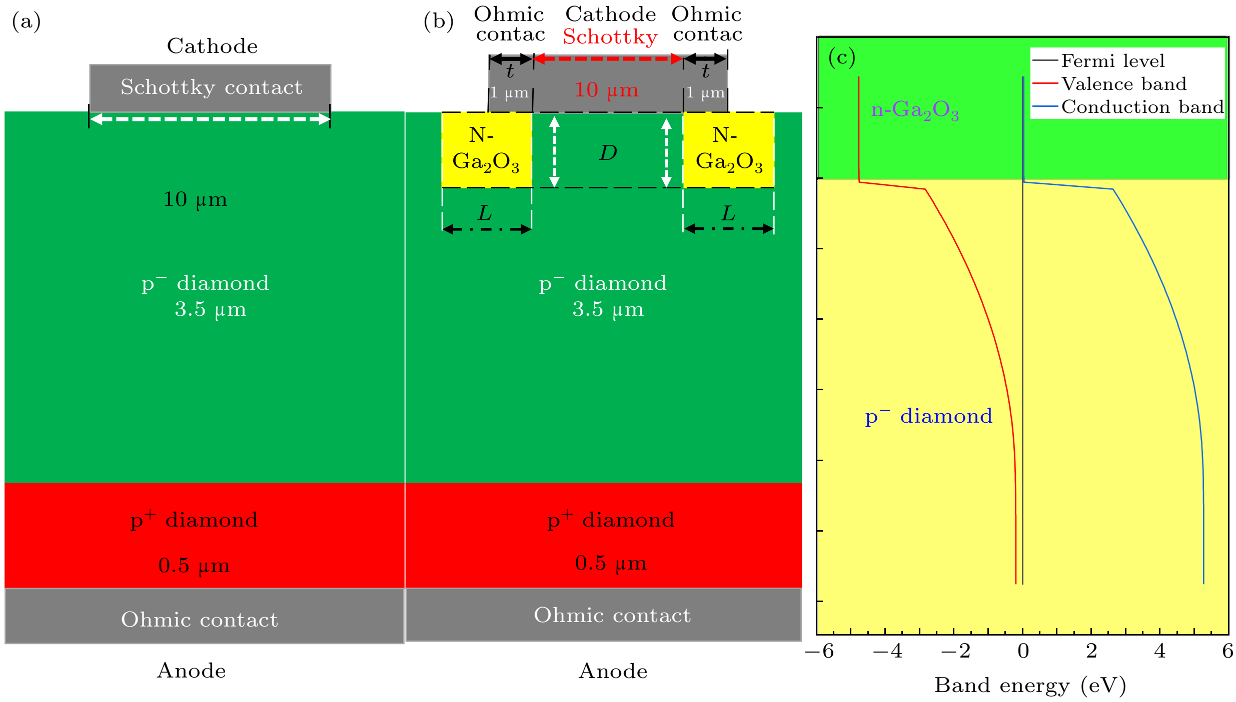

Fig. 1. Schematic structures of the vertical diamond SBDs (a) without and (b) with n-Ga_2O_3 JTE; (c) energy band diagram along the heterojunction interface with the doping concentrations of Ga_2O_3 and diamond being 1×10^{18} cm^{-3} and 1×10^{16} cm^{-3}, respectively.

3. Results and discussion

3.1. Effect of n-Ga_2O_3 JTE on the electrical properties

The depletion region introduced by the n-Ga_2O_3/p-diamond heterojunction plays a key role in the device performance. First, an n-Ga_2O_3 doping concentration of 1×10^{18} cm^{-3} and a JTE length of 3.5 μm were chosen for the simulation. Depths of 50 nm, 100 nm, 150 nm, and 200 nm were adopted for comparison with the diode without JTE (0 nm). The simulated electrical characteristics are shown in Table 3. The obtained I–V curves of the SBDs with different JTE lengths are shown in Fig. 2(a). When compared with the reference diode (0 nm), the turn-on voltages (V_{on}) are comparable for all the SBDs. However, the current density decreases obviously due to increasing R_{on} (Table 3). On the basis of the forward current distributions in Fig. 3, the depletion region in n-Ga_2O_3 suppresses the conduction path and increases the total diode area, resulting in the increase of R_{on} from 0.97 mΩ·cm^2 to 1.68 mΩ·cm^2 (Table 3).

Table 3. Simulated electrical characteristics of the SBDs with different JTE depths.

Conc. (10^{18} cm^{-3})	Length (μm)	Depth (nm)	V_{on} (V)	R_{on} (mΩ·cm^2)	V_{BD} (V)	BFOM (GW/cm^2)
1	3.5	0	2.64	0.97	200	0.04
1	3.5	50	2.62	1.62	750	0.30
1	3.5	100	2.61	1.68	1300	1.00
1	3.5	150	2.61	1.66	1350	1.10
1	3.5	200	2.60	1.68	1300	1.00

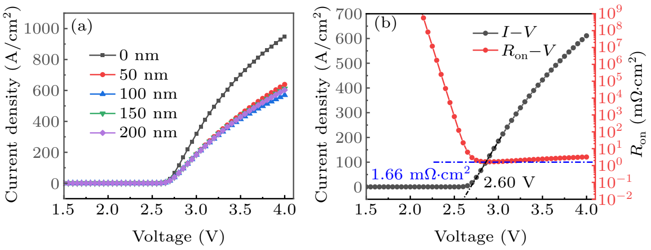

Fig. 2. (a) The I–V curves of the SBDs with different Ga_2O_3 depths; (b) typical I–V curve and the corresponding R_{on} for an n-Ga_2O_3 depth of 150 nm.

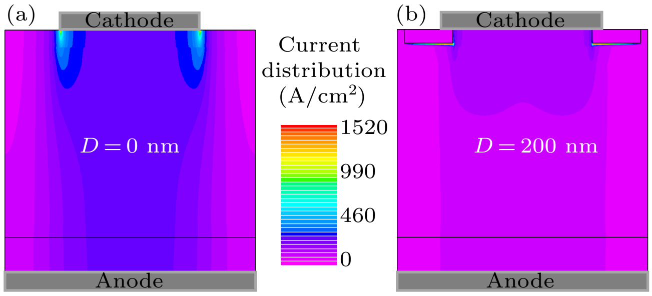

Fig. 3. Current distributions of the vertical diamond SBDs (a) without and (b) with 200-nm n-Ga_2O_3 JTE under a forward bias of 3 V.

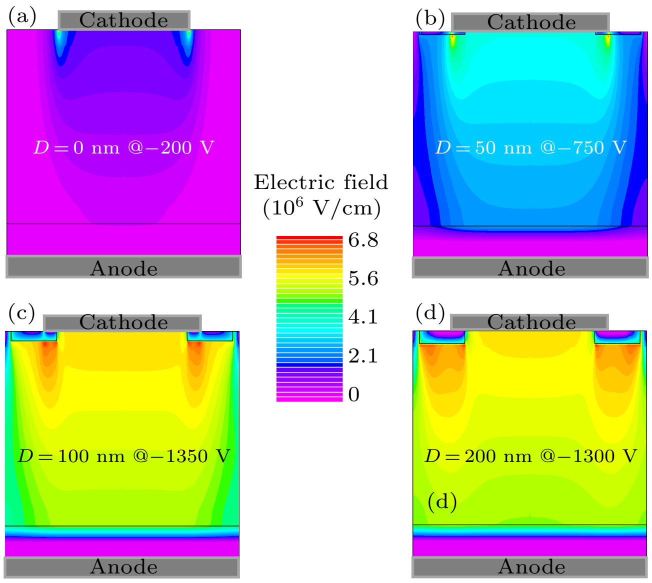

Fig. 4. Electric field distributions under V_{BD} for the vertical diamond SBDs with JTE depths of (a) 0 nm, (b) 50 nm, (c) 150 nm, and (d) 200 nm.

From Table 3, the R_{on} values of the SBDs with different depths of n-Ga_2O_3 are comparable to each other but V_{BD} (the electric field reaches 6 MV/cm) first increases and then decreases with increasing depth. The highest V_{BD} and BFOM value are 1350 V and 1.10 GW/cm^2 for the SBD with a JTE depth of 150 nm. From the electric field distribution at V_{BD}, obvious crowding effect occurs at the edge of the electrode for the SBD without JTE (Fig. 4(a)). After the introduction of JTE, the depletion regions in n-Ga_2O_3 and p-diamond sustain the reverse bias. Then, the electric field is distributed more even and broader, which is beneficial to realizing higher V_{BD} (Figs. 4(b) and 4(c)). However, the electric field tends to concentrate beneath n-Ga_2O_3 with the peak field occurring at the edge of JTE when the depth increases to 200 nm, resulting in the decrease of V_{BD} (Fig. 4(d)). The variation in the electric field distribution is also confirmed from the profiles shown in Fig. 5.

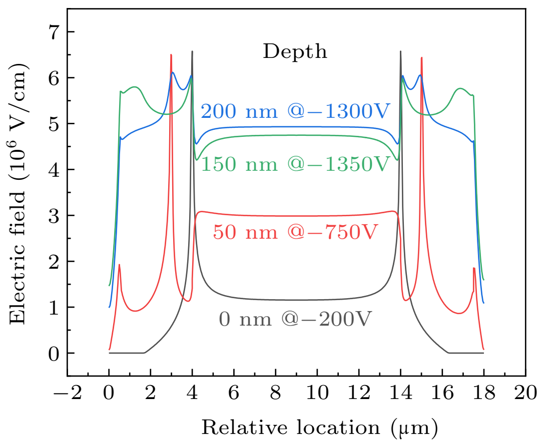

Fig. 5. Electric field profiles under V_{BD} for the vertical diamond SBDs with JTE depths of 0 nm, 50 nm, 150 nm, and 200 nm.

3.2. Optimization of the doping concentration of n-Ga_2O_3

To search the best doping concentration of n-Ga_2O_3, the effect of doping concentration on the electrical characteristics is studied. Doping concentrations of n-Ga_2O_3 of 1×10^{17} cm^{-3}, 5×10^{17} cm^{-3}, 1×10^{18} cm^{-3}, and 5×10^{18} cm^{-3} were selected with the depth and length of n-Ga_2O_3 being 150 nm and 2.5 μm, respectively. The simulation results are shown in Table 4.

Figure 6(a) shows the forward-biased I–V curves of the SBDs with different doping concentrations of n-Ga_2O_3. The figure demonstrates that the current densities and V_{on} values are comparable for all the SBDs, implying that the forward conduction is determined by the Schottky contact. The V_{on} and R_{on} of the SBDs are deduced from the I–V curves and summarized in Table 4. By taking the SBD with a doping concentration of 1×10^{18} cm^{-3} as an example (Fig. 6(b)), V_{on} defined by a linear extrapolation method and R_{on} were calculated to be approximately 2.61 V and 1.47 mΩ·cm^2, respectively. From Table 4, although all the V_{on} values of the SBDs are nearly the same, R_{on} increases slightly with increasing doping concentration. The mechanism can be explained from the forward current distributions as shown in Fig. 7. The depletion region at the n-Ga_2O_3/p-diamond interface is widened at higher doping concentration, which will suppress the conduction area and increase R_{on} slightly. On the basis of the aforementioned results, 1×10^{18} cm^{-3} was chosen as the optimum concentration to obtain the highest BFOM value.

Table 4. Simulated results for the SBDs with different doping concentrations of n-Ga_2O_3.

Conc. (10^{18} cm^{-3})	Length (μm)	Depth (nm)	V_{on} (V)	R_{on} (mΩ·cm^2)	V_{BD} (V)	BFOM (GW/cm^2)
0.1	2.5	150	2.61	1.46	350	0.08
0.5	2.5	150	2.61	1.46	750	0.39
1	2.5	150	2.61	1.47	1150	0.89
5	2.5	150	2.61	1.48	500	0.17

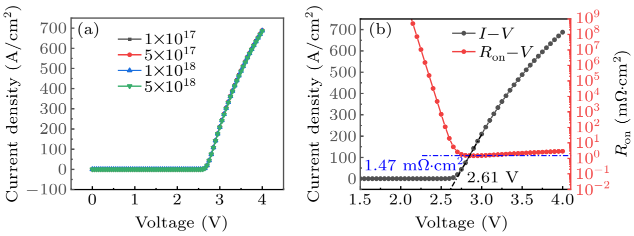

Fig. 6. (a) The *I–V* curves of the SBDs with different doping concentrations of n-Ga_2O_3; (b) typical *I–V* curve and the corresponding R_{on} for a doping concentration of 1×10^{18} cm^{-3}.

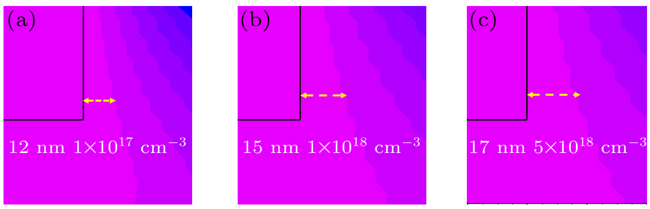

Fig. 7. Depletion region width at the junction interface under different doping concentrations of n-Ga_2O_3.

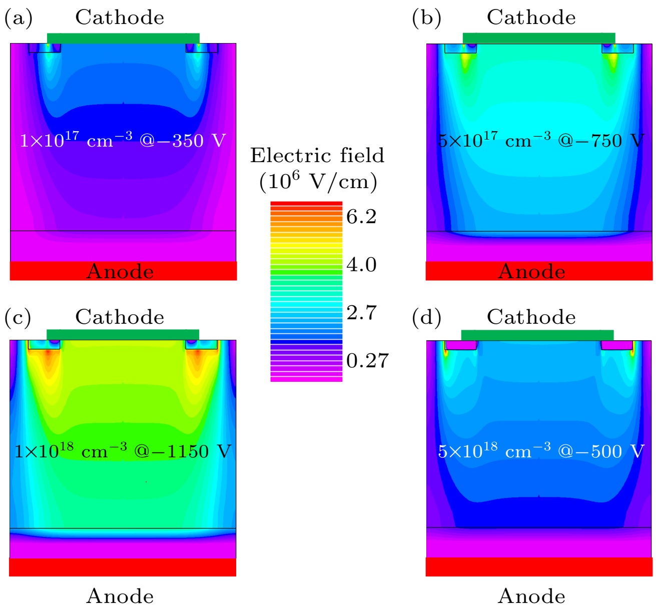

Fig. 8. Electric field distributions under V_{BD} for the vertical diamond SBDs with doping concentrations of (a) 1×10^{17} cm^{-3}, (b) 5×10^{17} cm^{-3}, (c) 1×10^{18} cm^{-3}, and (d) 5×10^{18} cm^{-3}.

The variation in V_{BD} versus the doping concentration was also evaluated, as shown in Fig. 8. The figure demonstrates that the n-Ga_2O_3 layer is totally depleted at the edge of the cathode when the doping concentration is 1×10^{17} cm^{-3}, resulting in a relatively low V_{BD}. The depletion region with a high doping concentration extends the electric field distribution and separates the peak into two parts, namely the edges of n-Ga_2O_3 and the cathode electrode. However, the dominant electric field peak shifts to the edge of n-Ga_2O_3 for a doping concentration of 5×10^{18} cm^{-3}. This can be attributed to the depletion region in n-Ga_2O_3 being too narrow to sustain the reverse voltage. The variation in the electric field distribution is also confirmed from the profiles shown in Fig. 9.

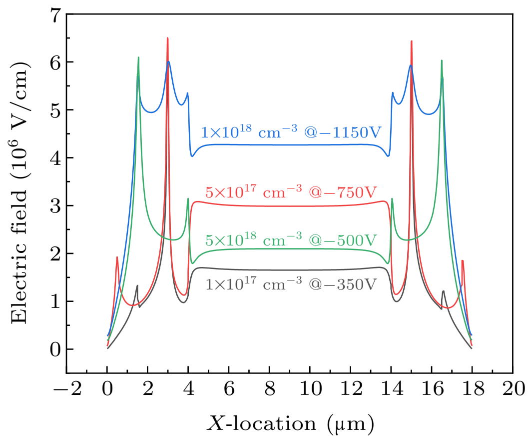

Fig. 9. Electric field profiles under V_{BD} for the vertical diamond SBDs with different doping concentrations of n-Ga_2O_3.

3.3. Optimization of the JTE length

Here, a doping concentration of 1×10^{18} cm^{-3} and a depth of 150 nm are chosen to evaluate the effect of JTE length on the device performance. The simulated electrical characteristics are summarized in Table 5, and the obtained *I–V* curves of the SBDs with different JTE lengths are shown in Fig. 10(a). It demonstrates that the V_{on} values are comparable for all the SBDs, whereas the current density decreases with increasing length. The introduction of JTE increases the total diode area and then increases R_{on} from 0.97 mΩ·cm^2 to 1.66 mΩ·cm^2 (Table 5).

Table 5. Simulated electrical characteristics of the SBDs with different JTE lengths.

Conc. (10^{18} cm^{-3})	Length (μm)	Depth (nm)	V_{on} (V)	R_{on} (mΩ·cm^2)	V_{BD} (V)	BFOM (GW/cm^2)
1	0	150	2.64	0.97	200	0.04
1	1.5	150	2.62	1.27	750	0.44
1	2	150	2.62	1.37	1000	0.73
1	2.5	150	2.62	1.47	1150	0.90
1	3	150	2.61	1.61	1250	0.97
1	3.5	150	2.60	1.66	1350	1.10

On the other hand, it can be observed that the reverse V_{BD} increases from approximately 200 V to 1350 V when the length increases to 3.5 μm. The calculated BFOM values presents a maximum of 1.10 GW/cm^2 for the SBD with a JTE length of 3.5 μm. The electric field distribution under the reverse bias region is also simulated to determine the mechanism of the JTE length (Fig. 11). When the doping concentration in the JTE is 1×10^{18} cm^{-3}, the depletion regions in both Ga_2O_3 and diamond sustain the reverse bias. Therefore, the electric field distribution is extended with increasing JTE length, resulting in enhanced V_{BD}.

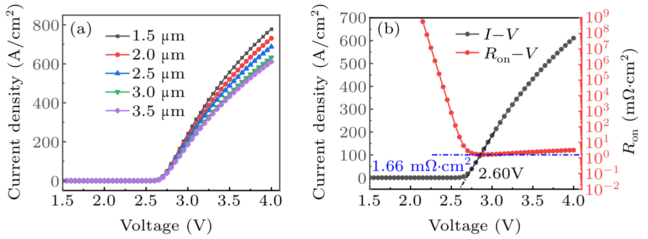

Fig. 10. (a) The I–V curves of the SBDs with different JTE lengths; (b) typical I–V curve and the corresponding R_{on} for a length of 3.5 μm.

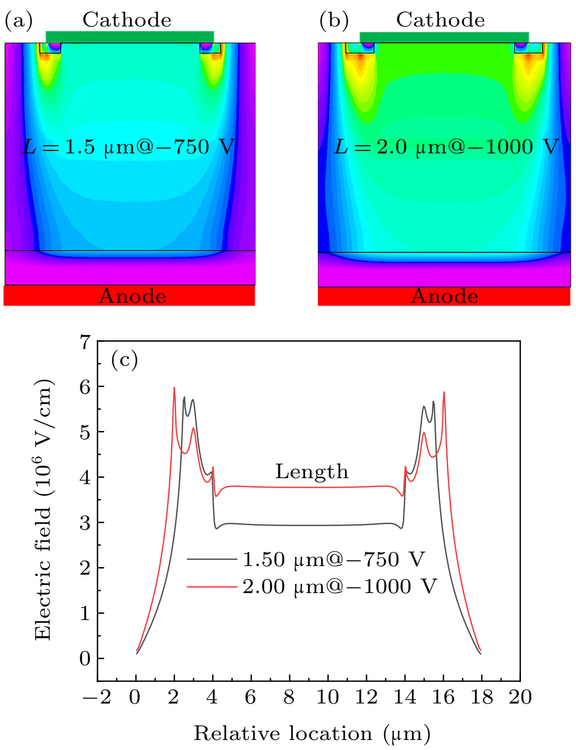

Fig. 11. [(a), (b)] Electric field distributions and (c) profiles under V_{BD} for the vertical diamond SBDs with JTE lengths of 1.5 μm and 2.0 μm.

3.4. Effect of work functions of the Schottky electrodes

On the basis of the prior discussion, the optimum length, depth, and doping concentration of the n-Ga_2O_3 region have been obtained. However, the V_{on} of the diode is relatively high, which requires a trade-off between V_{on} and V_{BD}. Generally, V_{on} presents a direct relationship with Schottky barrier height, which can be effectively modulated by a work function. Different cathode electrode materials (work functions) are chosen for further evaluation. The corresponding electrical characteristics are summarized in Table 6. The electrode material (work functions) has no obvious effect on V_{BD}. By considering the material properties, cost, and device parameters given in Table 6, we think that Al and Cu are the preferable electrode materials, which are also compatible with the conventional Si CMOS process.

Table 6. Simulated electrical characteristics of the SBDs with different Schottky electrode materials.

Conc. (10^{18} cm^{-3})	Length (μm)	Depth (nm)	Workf (eV)	V_{on} (V)	R_{on} (mΩ·cm^2)	V_{BD} (V)	BFOM (GW/cm^2)
1	3.5	150	3.66 (Mg)	2.99	1.55	1350	1.18
1	3.5	150	4.00 (Ref.)	2.61	1.66	1350	1.10
1	3.5	150	4.28 (Al)	2.38	1.74	1350	1.05
1	3.5	150	4.65 (Cu)	2.00	1.79	1350	1.02
1	3.5	150	5.10 (Au)	1.55	1.82	1350	1.00
1	3.5	150	5.56 (Pt)	0.98	1.84	1350	0.99

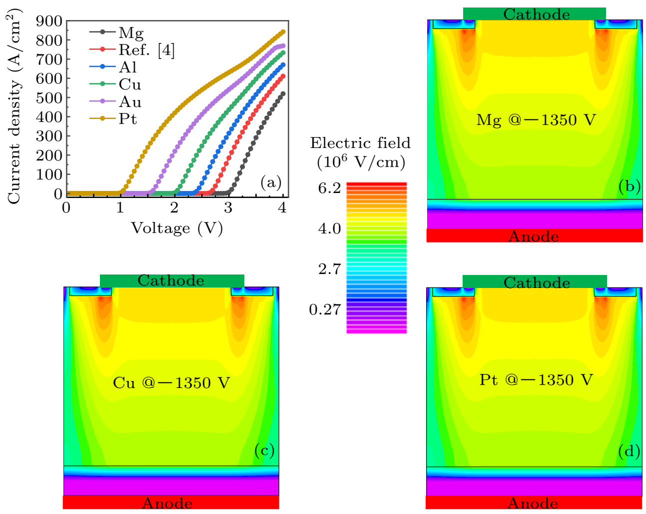

Fig. 12. (a) The I–V curves of the SBDs with different Schottky electrode materials; electric field distributions of (b) Mg, (c) Cu, and (d) Pt at a reverse voltage of 1350 V.

4. Conclusions and perspectives

Vertical diamond SBDs with and without an n-Ga_2O_3 JTE structure were proposed and simulated by Silvaco TCAD. The introduction of n-Ga_2O_3 JTE decreases the forward current density while enhancing the reverse breakdown voltage effectively with a medium depth of 150 nm. In addition, R_{on} increases slightly with increasing doping concentration of n-Ga_2O_3 while the electric field is distributed more even and broader. However, the depletion region in n-Ga_2O_3 is too narrow to sustain the reverse voltage when the doping concentration is higher than 5×10^{18} cm^{-3}. Furthermore, the electrical characteristics of the SBD can be enhanced with a large JTE length but with the increasing device area. Finally, Al and Cu were chosen as the preferable electrode materials to balance the forward turn-on voltage and the reverse breakdown voltage.

Acknowledgments

Project supported by the Key Research and Development Program of Guangdong Province, China (Grant

No. 2020B0101690001) and the Natural Science Foundation of Sichuan Province, China (Grant No. 2022NSFSC0886).

References

[1] Isberg J, Hammersberg J, Johansson E, Wikström T, Twitchen D J, Whitehead A J, Coe S E and Scarsbrook G A 2002 *Science* **297** 1670

[2] Umezawa H 2018 *Mater. Sci. Semicond. Process.* **78** 147

[3] Baliga B J 1989 *IEEE Electron Dev. Lett.* **10** 455

[4] Tolbert L M, Ozpineci B, Islam S K and Chinthavali M S 2003 *Semiconductors*

[5] Kubovic M, El-Hajj H, Butler J E and Kohn E 2007 *Diam. Relat. Mater.* **16** 1033

[6] Makino T, Tanimoto S, Hayashi Y, Kato H, Tokuda N, Ogura M, Takeuchi D, Oyama K, Ohashi H, Okushi H and Yamasaki S 2009 *Appl. Phys. Lett.* **94** 262101

[7] Teraji T, Koizumi S, Koide Y and Ito T 2007 *Jpn. J. Appl. Phys.* **46** L196

[8] Umezawa H, Nagase M, Kato Y and Shikata S I 2012 *Diam. Relat. Mater.* **24** 201

[9] Traoré A, Muret P, Fiori A, Eon D, Gheeraert E and Pernot J 2014 *Appl. Phys. Lett.* **104** 052105

[10] Zhao D, Hu C, Liu Z, Wang H X, Wang W and Zhang J 2017 *Diam. Relat. Mater.* **73** 15

[11] Lei Y, Shi H, Lu H, Chen D, Zhang R and Zheng Y 2013 *J. Semicond.* **34** 054007

[12] Wang Y, Li Z Y, Hao Y, Luo X, Fang J P, Ma Y C, Yu C H and Cao F 2018 *IEEE Trans. Electron Dev.* **65** 2552

[13] Ma J, Zanuz D C and Matioli E 2017 *IEEE Electron Dev. Lett.* **38** 1298

[14] Allen N, Xiao M, Yan X, Sasaki K, Tadjer M J, Ma J, Zhang R, Wang H and Zhang Y 2019 *IEEE Electron Dev. Lett.* **40** 1399

[15] Yu X, Zhou J, Wang Y, Qiu F, Kong Y, Wang H and Chen T 2019 *Diam. Relat. Mater.* **92** 146

[16] Lin C H, Yuda Y, Wong M H, Sato M, Takekawa N, Konishi K, Watahiki T, Yamamuka M, Murakami H, Kumagai Y and Higashiwaki M 2019 *IEEE Electron Dev. Lett.* **40** 1487

[17] Han S, Yang S and Sheng K 2019 *IEEE Electron Dev. Lett.* **40** 1040

[18] Gupta S K, Shekhar C, Akhtar J and Pradhan N 2012 *IEEE Trans. Semicond. Manuf.* **25** 664

[19] Driche K, Rugen S, Kaminski N, Umezawa H, Okumura H and Gheeraert E 2018 *Diam. Relat. Mater.* **82** 160

[20] Sun X, Guo Y, Wu G, Zhao Y, Liu S and Li H 2020 *Diam. Relat. Mater.* **108** 107924

[21] Kato H, Yamasaki S and Okushi H 2007 *Diam. Relat. Mater.* **16** 796

[22] Mishra A, Abdallah Z, Pomeroy J W, Uren M J and Kuball M 2021 *IEEE Trans. Electron Dev.* **68** 5055

[23] Xiong W H, Zhou X Z, He Q M, Jian G Z, Chen C, Yu Y T, Hao W B, Xiang X Q, Zhao X L, Mu W X, Jia Z T, Tao X and TandLong S B 2021 *IEEE Electron Dev. Lett.* **42** 430

[24] Wang Q L, Fu S Y, He S H, Zhang H B, Cheng S H, Li L A and Li H D 2021 *Chin. Phys. B* **31** 088104

[25] Wang T T, Li X, Pu T, Cheng S, Li L, Wang Q, Li H and Ao J P 2021 *Superlattices Microstruct.* **159** 107048

[26] Zhou X Z, Liu Q, Xu G W, Zhou K, Xiang X Q, He Q M, Hao W B, Jian G Z, Zhao X L and Long S B 2021 *IEEE Trans. Electron Dev.* **68** 1501

[27] Donato N, Antoniou M, Napoli E, Amaratunga G and Udrea F 2015 *Proc. Int. Semicond. Conf. CAS* **2** 223

[28] Nandi A, Rana K S and Bag A 2021 *IEEE Trans. Electron Dev.* **68** 6052